

Controlling topological defects and contractile flow in confined nematic cell population

Ryo Ienaga,¹ Kazusa Beppu,^{1,2} and Yusuke T. Maeda^{1,*}

¹*Department of Physics, Kyushu University, Motoooka 744, Fukuoka 819-0395, Japan*

²*Department of Applied Physics, Aalto University School of Science, Puumiehenkuja 2, Espoo, 02150, Finland*

(Dated: December 29, 2022)

Topological defects in an orientation field play a vital role for controlling the collective motion of nematic cell populations within epithelia and tissue. In this study, we study the geometric control of the collective motion in a nematic cell population to further explore the interplay between topology and dynamics in active nematics. By applying spatial constraints consisting of two or three overlapping circle boundaries, we demonstrate an ordered pairing of half-integer topological defects in a confined cell population. The defects facing each other can induce a contractile cellular flow at broad geometric conditions. This robust contractile flow contributes to mechanical stimulation while altering the cell nucleus, which may be relevant to geometry-dependent morphogenesis.

Introduction

Understanding the self-organized structure and dynamics is a central issue in the physics of non-equilibrium systems. In recent years, the ordered collective motion of active matter that moves with consuming chemical energy has been extensively studied to explore the physical principle and applied engineering approach involved in complex biological systems [1–3]. Active nematics is one class of active matter with no front-back asymmetry in the orientation interaction [4]. They show a nematically organized orientation field in various biological systems, such as dense bacterial colonies [5, 6], cytoskeletons and molecular motors complexes [7, 8], nematic cell population [9–15], and the hydra morphogenesis [16].

Nematic interacting particles or cells are locally oriented to form an ordered orientation field in two-dimensional space, but there are singularities where the orientation cannot continuously change, and nematic order is broken locally. These elements are called topological defects that can be created or annihilated to govern the structure and mechanics of materials. For nematic liquid crystals, rod molecules are misaligned in a defect with orientation and a topological charge. However, what makes active nematics differ from passive nematic liquid crystals is the spontaneous motion of the defects coupled with spontaneous collective motion [4, 9, 11, 12]. For an important aspect of biological systems, topological defects in the nematic cell populations alter the local cell density by trapping or depleting cells with asymmetric frictional interactions [13, 14]. While our understanding of collective motion in the vicinity of defects has been extensively advanced, developing a means to control the position of defects is still little explored to further pursue the interplay of topology and dynamics in active nematics.

One promising way to control the collective motion of active matter is through geometric control of the boundary geometry. Past studies have shown that a dense bacterial suspension shows active turbulent motion, but by

enclosing this dense suspension in spatial confinements, the vortex rotation inherent in turbulence is extracted [17]. Furthermore, by making ordered bacterial vortices interact with each other, one can control the pairing pattern of rotating vortices in a geometrically designed manner [18–21]. Although there is growing evidence that the shape of the boundary is key to organizing the emergent structure of active cytoskeleton [22], cell monolayer [23–27] and myoblast cell morphogenesis [28, 29], the geometric control of topological structure is still elusive.

In this study, we aim to develop a physical strategy for controlling active nematics with a geometric design of spatial confinement. We built a microfabrication method that allows nematic cell populations to move only in a spatial constraint with a designed boundary shape. This confinement can control the positioning of defects in the orientation field while keeping the net topological charge. We found that the ordered pairing of the defects induces the emergent contractile flow toward the geometric center of the confined cell population at broad geometric parameters. Such contractile flow can exert mechanical stress on the group of cells, suggesting that the defect pairing may contribute to force-induced differentiation of the myoblast population.

Results

First, we investigate the collective motion and associated orientation dynamics of myoblast C2C12 cell population on a flat two-dimensional surface $\mathbf{x} = (x, y)$. The cultured cells have spindle-like cell morphology, and their polarized cell shape allows them to align the orientation heading angle through interaction with neighbor cells. Cell-cell adhesion is not strong in C2C12 cells, which suggests that their intercellular interaction is nematic interaction. The cells were grown in a culture dish, and their collective motion was recorded by time-lapse acquisition at 10 min intervals for 48 hours. Initially, the cell population is little organized in their orientation, and singular points with local orientation gaps are distributed (FIG.

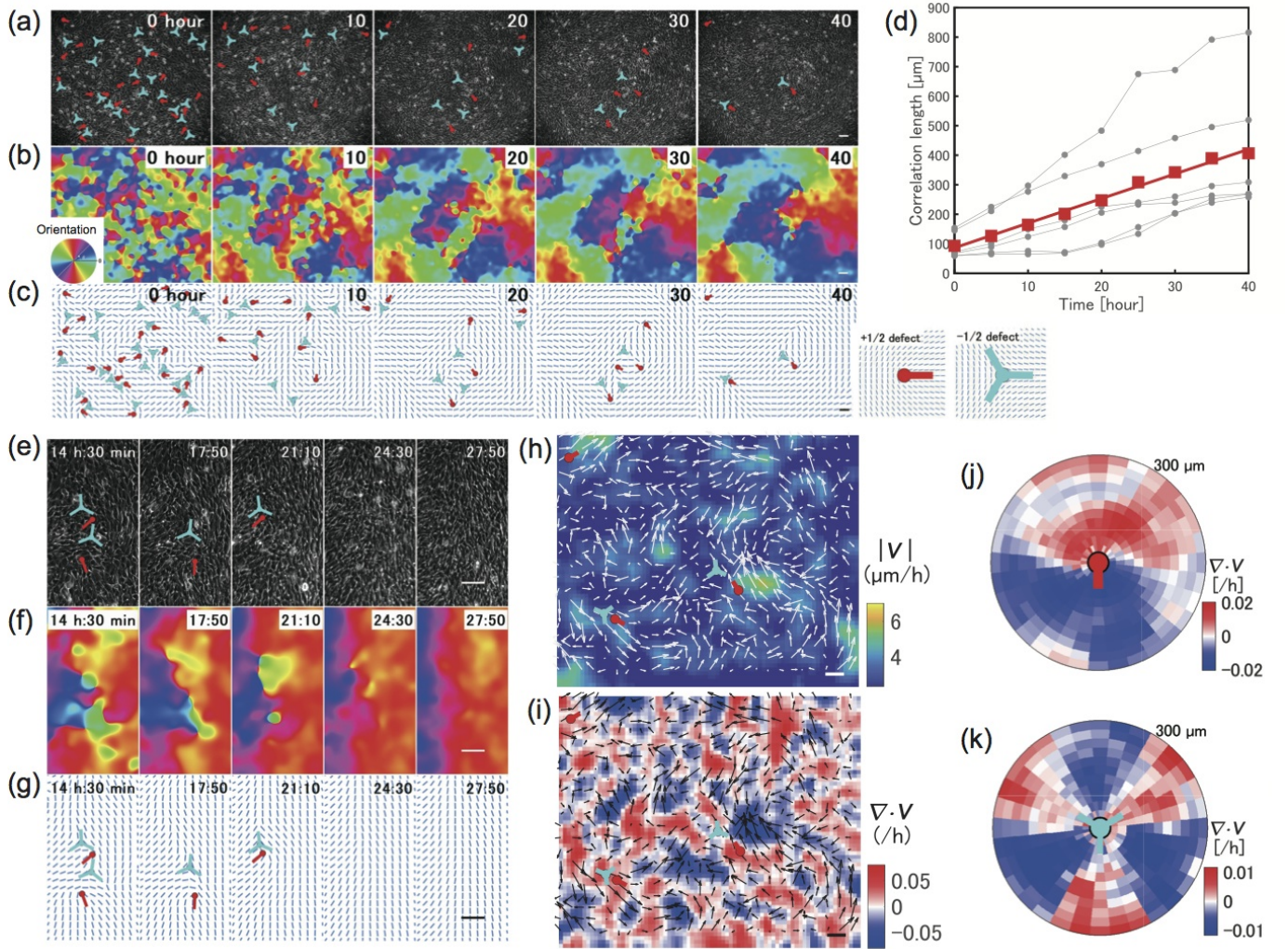


FIG. 1. Collective motion and ordered orientation dynamics of myoblast cell (C2C12 cell) population. Scale bars: 100 μm . **(a-c)** Collective motion and orientation dynamics of C2C12 cell population on a two-dimensional flat surface. The red symbol represents $+1/2$ topological defects, and the blue represents $-1/2$ topological defects. **(a)** Phase contrast images. **(b)** The orientation field analyzed from (a). Color decodes the orientation field. **(c)** Corresponding director field analyzed from (a). **(d)** Time evolution of correlation length of orientation field. Thin black lines represent the correlation length calculated from single experiments. Red dots represent the mean value and solid line is a fitting curve. **(e-g)** Annihilation of topological defects in C2C12 cell population. **(e)** Phase contrast images. **(f)** The orientation field analyzed from (e). **(g)** Corresponding director field analyzed from (e). **(h)** The speed $|\mathbf{v}|$ of collective motion of C2C12 cell population. The velocity field \mathbf{v} is obtained from PIV analysis of phase contrast images. **(i)** The velocity divergence, $\nabla \cdot \mathbf{v}$. **(j)** Spatial profile of the divergence of velocity field near $+1/2$ topological defect. **(k)** Spatial profile of the divergence of velocity field near $-1/2$ topological defect.

1(a), $t=0$ h). Such singularity, known as topological defects, include the $+1/2$ topological defect, in which the orientation phase deviates by $+\pi$, and the $-1/2$ defect, in which the orientation deviation is $-\pi$. These half-integer topological defects are present in approximately equal numbers but seem to be distributed irregularly in space at the earlier time (FIG. 1(a)-(c)). These topological defects spontaneously move with cell motion, and their position and number change over time due to annihilation. Then, the orientation of the cells gradually aligns and leads to the expansion of orientation correla-

tions. To investigate the growth of nematic alignment order, we analyzed the time evolution of the correlation length of the orientation field. As shown in FIG. 1(d), the correlation length increases proportionally with time. Moreover, we observed the spontaneous annihilation of $+1/2$ and $-1/2$ defects approaching each other when these half-integer defects collide at specific orientations. Their annihilation aligns cellular orientation over long distances (FIG. 1(e)-(g)), consistent with the fact that the region of aligned orientation is expanded over time. Thus, the pair of moving topological defects is key to organizing

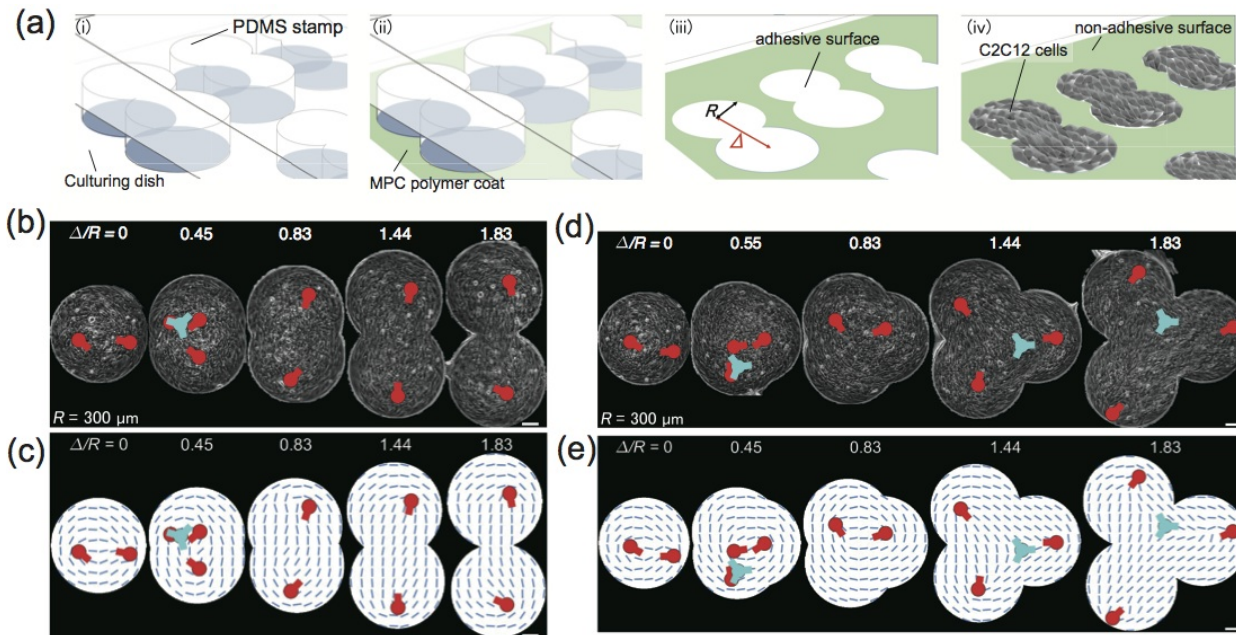


FIG. 2. Patterning C2C12 cell population in confined overlapped circles and controlling topological defects pairing. The red symbol represents $+1/2$ defect and the blue symbol $-1/2$ defect, respectively. Scale bars: $100\ \mu\text{m}$. (a) Schematic illustration of microfabrication steps. Step (i) Adheres the poly-dimethyl siloxane (PDMS) stamp weakly to the culture dish. Step (ii) Coating of MPC polymer. Step (iii) Make the designed adhesive region by removing the PDMS stamp. Step (iv) Spread the C2C12 cells on the designed pattern and grow inside the adhesive region. (b and c) Phase contrast images of confined C2C12 cells. The confined C2C12 cells in (b) overlapped doublet circle pattern and (c) triplet circle pattern. The geometric parameters are $\Delta/R = 0, 0.45, 0.83, 1.44,$ and 1.83 . (d and e) The director fields of confined C2C12 cells analyzed from (b) and (c). The local director patterns denote the localization of topological defects in confined geometries.

the orientation field of the C2C12 cell population.

What makes active nematics differ from passive liquid crystal is the interplay of orientation field with collective motion. It has been reported that the collective motion around a topological defect is driven by active force associated with the orientation field. To clarify the interplay between topological structure and the velocity field of collective motion, we calculated the velocity field of collective motion $\mathbf{v}(\mathbf{x})$ by PIV analysis. The speed of collective motion $|\mathbf{v}|$ was higher in the vicinity of $+1/2$ topological defects (FIG. 1(h)), but there was no clear indication of a global pattern in the velocity field. From the active motion close to $+1/2$ defect, velocity divergence $\nabla \cdot \mathbf{v}$ was calculated to analyze the locally organized pattern of the velocity field (FIG. 1(i)). A characteristic structure appears in the velocity divergence near the topological defects. We found that the sign of the divergence reverses at the $+1/2$ defect, i.e., the flow field that flows out toward the defect is stabilized (FIG. 1(j)). Furthermore, the $-1/2$ defect shows three-fold symmetric velocity divergence, which is consistent with the fact that the orientation around the defect has three-fold symmetry (FIG. 1(k)), meaning that the collective motion of C2C12 cells follows the topological structure of the orientation field.

We next designed a geometrically controlled pairing ar-

rangement of topological defects to understand the mechanism by which long-range orientation order emerges in C2C12 population. We imposed geometric confinement to C2C12 cells and used the reverse micro-contact printing method on the flat surface (FIG. 2(a), see Materials and Methods). The boundary of confined space is defined as the doublet or triplet circle geometry where the two or three circles with the same radius R overlap at a distance Δ . We analyzed the collective motion of confined C2C12 cells with various geometric parameters $\Delta/R = 0, 0.15, 0.25, 0.35, 0.45, 0.55, 0.65, 0.83, 1.44,$ and 1.83 and the confinement radius $R = 200, 250, 300$ and $350\ \mu\text{m}$.

By analyzing the bright-field images of a confined cell population, we found the cellular orientation shows a bipolar-like orientation pattern in which the cells align in the long axis direction of the doublet circle (FIG. 2(b)). Confined C2C12 cells had one $+1/2$ topological defect clearly located within one circular compartment as the distance between the centers of the circles Δ increased at the constant radius R . The two $+1/2$ defects were arranged along the long axis in a pattern facing each other (FIG. 2(c)), indicating that a nematic-like ordered pattern is realized under the geometrical shape. Similarly, in the triplet circular boundary, in which three circles overlap, the cells show three-fold symmetry and a trifurcated branching orientational pattern connecting the

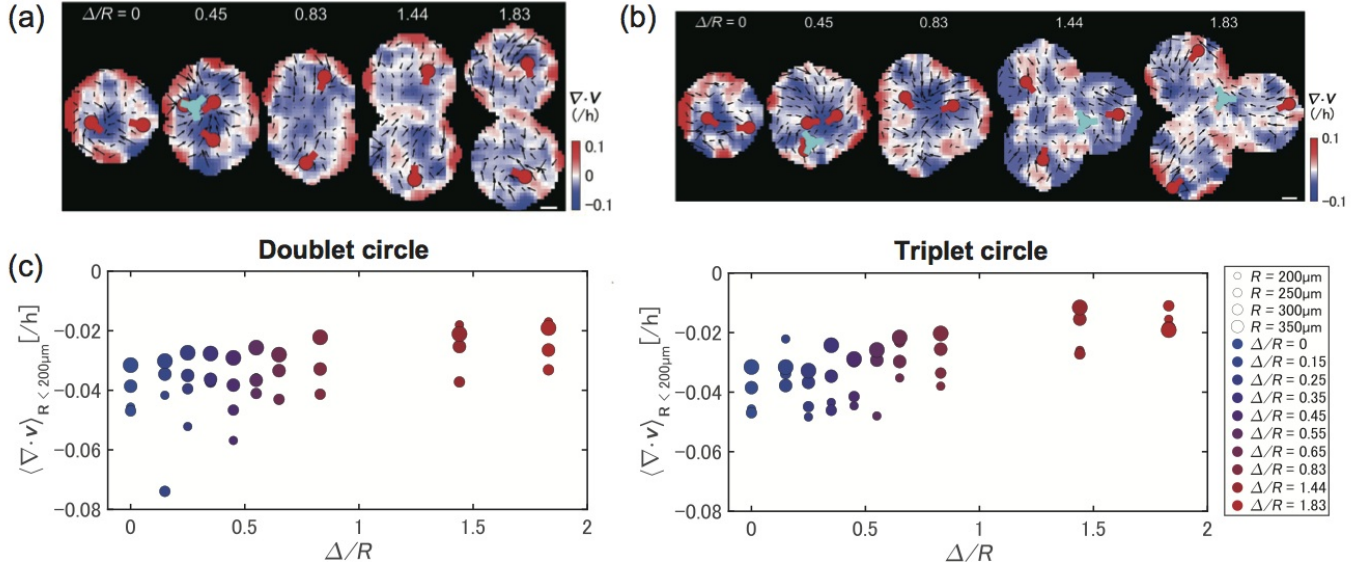


FIG. 3. **Ordered collective motion with topological defects pairing in confined C2C12 cells.** Scale bars: 100 μm . (a and b) Velocity divergence, $\nabla \cdot \mathbf{v}$, of confined C2C12 cells. The cell population is confined in (a) doublet circle boundary and (b) triplet circle boundary with the geometric parameters $\Delta/R = 0, 0.45, 0.83, 1.44, \text{ and } 1.83$. (c) The velocity divergence $\nabla \cdot \mathbf{v}$ in confined C2C12 cells in doublet circle boundary (left) and triplet circle boundary (right). We calculated the average velocity divergence in the radius $R = 200, 250, 300$ and $350 \mu\text{m}$ and in ten patterns of geometric parameters $\Delta/R = 0, 0.15, 0.25, 0.35, 0.45, 0.55, 0.65, 0.83, 1.44, \text{ and } 1.83$.

centers of the circles (FIG. 2(d)). Three-fold symmetry appeared with one $+1/2$ defect in each circle as Δ/R increased (FIG. 2 (e)). Furthermore, because C2C12 cells are confined to a single closed space, the net topological charge is considered to become $+1$ in energy minimization. Therefore, the three $+1/2$ defects were arranged to face each other, and one $-1/2$ defect was located at their intersection (FIG. 2 (e)). In particular, the $-1/2$ defect was placed close to the geometric center of the constraint region, forming a basis of three-fold symmetry.

Furthermore, topological defects in active nematics can spontaneously move, and this motion often causes the annihilation of defects, resulting in the expansion of the aligned orientation field (FIG. 1(a)-(c)). Indeed, there is a characteristic pattern in the collective motion around topological defects ($\nabla \cdot \mathbf{v}$ near $+1/2$ defect and $-1/2$ defect, FIG. 1(j) and (k)), representing a close link between the velocity field and the orientation dynamics of active nematics. It is a reasonable consideration that if the actively moving topological defects are fixed in space, directional collective motion is able to occur in the designed pattern of topological defects. Hence, by taking our geometric patterning in spatially constrained C2C12 cells, we investigate the velocity field of collective motion coupled with the defect pairing pattern.

In a doublet circle boundary, an inward flow from the boundary to the center is formed from $+1/2$ defects at any Δ/R (FIG. 3(a)). The same velocity pattern of collective motion from $+1/2$ defects near each circle's center

toward the geometric center also occurs in the triplet circular boundary (FIG. 3(b)), suggesting that the topological defects induce stabilization of the inward collective flow. Since $+1/2$ topological defects are located close to the center of each circular confinement facing each other, velocity divergence is mostly negative throughout the confined space in both the doublet and triplet circle boundaries (FIG. 3(c)). The mean value of the velocity divergence in the constrained space was negative regardless of the geometrical conditions Δ/R , indicating an inward contractile flow robustly heads to the center of the constrained region. Moreover, velocity divergence is larger for smaller constraint size R (FIG. 3(c)). This geometric dependence reflects that the collective motion in contractile flow decays over distance because only one $+1/2$ topological defect is placed in each circular region. Furthermore, the activity of the intracellular myosin molecular motor is the driving force for the motion of individual cells. We tested whether the myosin activity perturbation alters the contractile flow of the collective motion. The pairing of $+1/2$ defects was also built within the doublet circle boundary, and the negative velocity divergence was apparent on all Δ/R parameters even at reduced collective motion (FIG. S1). This means that the contractile flow pattern is robust to partial activity perturbation.

To further examine the collective motion near geometrically controlled topological defects, we record the trajectory of individual cell motion by nucleus tracking velocimetry analysis. SiR-DNA that labels cell nucleus

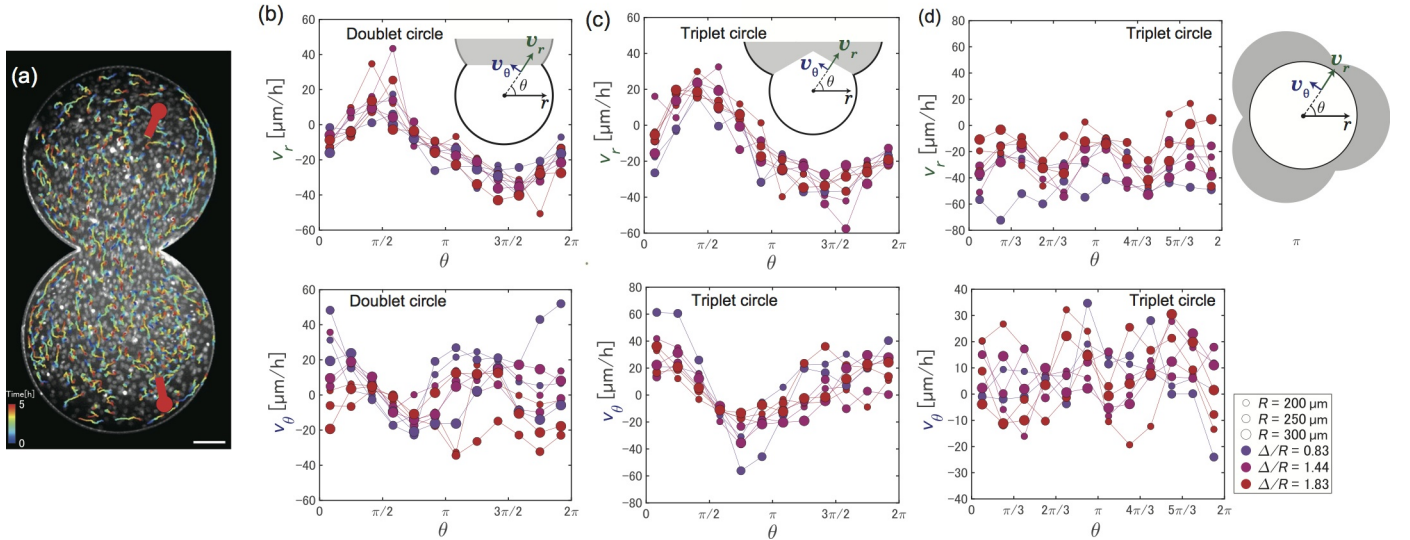


FIG. 4. **The contractile flow and angular dependence of collective motion** (a) The trajectories of tracked cell nucleus in confined C2C12 cells. SiR-DNA visualized the nucleus of individual cells. The color change of the trajectory represents time evolution. Scale bar: $100\mu\text{m}$. (b-d) The radial velocity (\mathbf{v}_r , top) and angular velocity (\mathbf{v}_θ , bottom) of cells analyzed from nucleus tracking. \mathbf{v}_r and \mathbf{v}_θ are averaged over a fan-shaped region of interest divided every 25° . (b) The velocity profiles in the doublet circle boundary. The center of one of the two overlapping circles is the origin of the polar coordinate $\mathbf{r} = (r, \theta)$. The angle θ is set so that the center of the other circle is on the extension line of $\theta = \pi/2$. The positive sign of \mathbf{v}_r indicates the cell nucleus moves away from the center of the circle. (c) The velocity profiles in the triplet circle boundary. The center of one of the three overlapping circles is the origin of the polar coordinate. θ is set so that the geometric center of three overlapping circles is on the extension line of $\theta = \pi/2$. (d) The velocity profiles in the center of the triplet circle boundary. The origin of the polar coordinate is set at the geometric center of overlapping three circles.

with low toxicity was used to track the motion of cell nucleus (FIG. 4(a)). In the doublet circle boundary, we define the polar coordinates $\mathbf{r} = (r, \theta)$ in each circle and the center of the circle is taken as the origin of the polar coordinate. We also define the angle θ so that the center of the other circle is on the extension line of $\theta = \pi/2$. The radial and angular velocity components, \mathbf{v}_r and \mathbf{v}_θ , represent the motion of the cell nucleus close to the topological defects (FIG. 4(b)).

The radial velocity \mathbf{v}_r has a clear angular dependence in the doublet circle boundary, moving at a faster speed outward from the center at an angle $\theta = \pi/2$ and moving at a faster rate toward the center at $\theta = 3\pi/2$. Such spatial profile in \mathbf{v}_r is commonly found in various geometric conditions Δ/R and the constraint radius R (FIG. 4(b)). Moreover, the angular velocity \mathbf{v}_θ also has angular dependence, moving at a slower speed in angle direction at $\theta = \pi/2$. Considering that a $+1/2$ defect is located near the origin as seen in FIG. 2(b) and heading at the direction at $\theta = \pi/2$, this angular dependence of cell motion means that individual cells move in the direction that $+1/2$ defects are facing each other, which is consistent with the contractile flow in collective motion (FIG. 3). In the triplet circle boundary, same angular dependence of \mathbf{v}_r and \mathbf{v}_θ present, indicating that the $+1/2$ topological defect promotes directional control of cell motion and has the property of inducing contractile flow of collective

motion toward the center of the confined space, regardless of the geometric parameters (FIG. 4(c)).

Not only for $+1/2$ defects but another $-1/2$ defect is also located near the geometric center of the triplet circle boundary (FIGs. 2 and 3). By defining the geometric center of the triplet circle boundary as the origin, we analyzed the \mathbf{v}_r and \mathbf{v}_θ of the cell nucleus moving near the $-1/2$ defect. We found the three-fold symmetry pattern in \mathbf{v}_r at $\Delta/R=1.44$ and 1.83 , reflecting the contractile flow emanating from three $+1/2$ defects located inside three circles. In contrast, no clear geometric dependence appeared in \mathbf{v}_θ (FIG. 4(d)), consistent with the fact that nematic cell interaction alone does not lead to the net angular flow within closed symmetric boundaries.

Finally, in order to explore biological relevance in cellular mechanics, we investigate how the contractile flow caused by the pair of topological defects affects cellular orientation. The velocity divergence, $\nabla \cdot \mathbf{v}$, changes with time, and the appearance of contractile flow becomes more apparent between the facing $+1/2$ defects at the doublet circle boundary (FIG. 5(a)). The C2C12 cells are moving by exerting contractile force, and the cell population collectively moves in an aligned orientation between $+1/2$ defects in the doublet boundary, which may be causing changes in microscopic shape such as nucleus morphology. To address this question, we analyzed the shape of the cell nucleus of confined C2C12 cells under

the geometric constraints at $\Delta/R = 1.83$ and $R=300\ \mu\text{m}$ (FIG. 5(b) and (c)). Using image processing, we examined the shape of the cell nucleus with the aspect ratio of the major length to the width (minor length). After visualizing the shape variation of each cell nucleus with the aspect ratio, we found that an elongated nucleus (i.e., high aspect ratio) can be mostly found around the midpoint of the pair of $+1/2$ defects in both doublet (FIG. 5(b)) and triplet boundary conditions (FIG. 5(c)). In addition, although the deformation of the nucleus was not large at the initial stage (Day-0), the larger deformations became more pronounced after about 48 hours (Day-2) in both doublet and triplet overlapping circles (FIG. 5(d) and (e)). This result indicates that the contractile flow occurring on the region between the two $+1/2$ defects facing each other exerts mechanical stimulation onto cells and stretches the cell nucleus.

Conclusion

In this study, we studied the collective motion induced by topological defects in myogenic stem cells C2C12. The orientation field of cell populations generates topological defects on a two-dimensional plane and the correlation length of orientation increases with time as $+1/2$ defects and $-1/2$ defects annihilate. We examined the control of defect positioning by enclosing C2C12 cells in a geometrical boundary where two or three circles overlapped. The C2C12 cells were found to form an orientation pattern with two $+1/2$ topological defects, three $+1/2$ topological defects, and one $-1/2$ defect in each boundary shape. The orientation pattern evolves to the most stable configuration with a net topological charge of $+1$, meaning that the symmetry of the geometrical boundaries determines induced topological defects and their locations under a confined region.

Moreover, we addressed elucidating the self-organization of collective motion induced by the pairing of topological defects. Assisted with the geometrically designed boundary conditions, the pairing of $+1/2$ defects induced the contractile flow of collective motion characterized by negative velocity divergence. This contractile flow occurs independently of the geometrical conditions of Δ/R . Our finding reveals how the alignment of cell orientation controls collective motion robustly in a geometrically constrained boundary.

Our findings also give new insights into myotube induction, as C2C12 cells are known to fuse into myotubes after culture induction. The deformation of the cell nucleus is induced with the increase in density, indicating that the cells are exposed to a large source of mechanical stimuli. It has recently been suggested that the deformation of the cell nucleus is also involved in controlling cell differentiation, such as increasing the contractile force of myosin molecular motors. The nucleus stretching un-

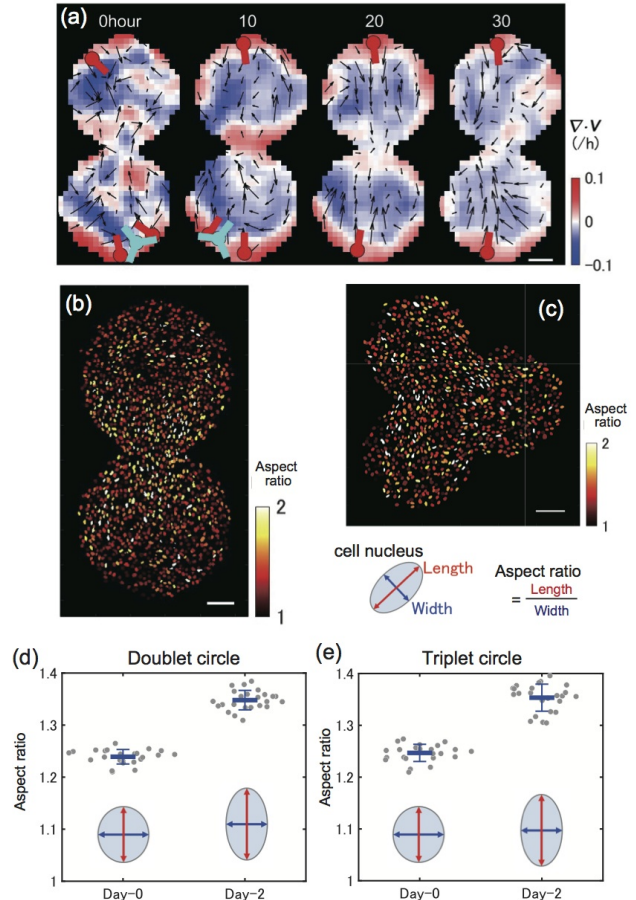


FIG. 5. **The deformation of cell nucleus under the pairing of topological defects.** Geometric parameters are $R=300\ \mu\text{m}$ and $\Delta/R=1.83$. Scale bars: $100\ \mu\text{m}$. (a) Representative time evolution of velocity divergence of confined cells in the doublet circle boundary. Scale bar: $100\ \mu\text{m}$. (b and c) The spatial map of the cell nucleus in the doublet circle boundary (b) and the triplet circle boundary (c). The representative fluorescent images taken at 48 hours are shown with color code for aspect ratio. The aspect ratio is defined as the ratio of major length (length) to minor length (width) of the cell nucleus. The large aspect ratio in white color indicates stretched nucleus shape. Cell nuclei with a high aspect ratio are found around the midpoint of the pair of $+1/2$ defects. (d and e) Temporal increase in aspect ratio of cell nuclei. The shape of cell nucleus at the start of the measurement (Day 0) is compared with that at $t=48$ hour (Day 2). The aspect ratio increases in both the doublet circle boundary (d) and the triplet circle boundary (e).

der the contractile flow may provide new insight into the mechanism of force-induced morphogenesis through the geometric control of actively moving topological defects.

Materials and Methods

Cell culture

C2C12 cells were cultured in MEM medium (20% FBS, Glutamax, Sodium pyruvate, and antibiotics) at 37°C and 5.0% CO₂. C2C12 cell suspension was spread in 35 mm glass-bottom dishes at initial density 1.5×10^5 cells/mL. The cell culture was incubated for 1 hour to allow the cells to attach to the substrate surface. For individual cell tracking, the cell nucleus was visualized by 250 nM SiR-DNA (CY-SC007, Cytoskeleton, Inc.).

Microfabrication

The patterning of the geometry of the cell adhesion region was created by reverse micro-contact printing of PDMS (Sylgard 184, Corning). First, a pattern with the geometry of the adhesion region was created with a PDMS device, and then plasma surface treatment was applied to adhere it to a glass bottom dish. The MPC polymer (Lipidure, NOF corporation) coating agent was poured into this area to form the non-adhesive area. Then, the PDMS device was peeled off to form the uncoated area where the cell could adhere to the substrate. The photomask for microfabrication was purchased from MITANI Micronics, and other conventional microfabrication protocols were described in previous studies [19, 20, 22].

Microscopy

Microscopic measurement was conducted using an epifluorescence microscope (IX73, Olympus) with CMOS camera (Zyla 4.0, Andor) and LED light source. The culture medium's temperature and CO₂ concentration were controlled at 37°C and 5.0%, respectively, by the stage-top incubator (STXG-IX3WX, TOKAI-Hit). The microscope stage is automatically position-controlled, and multi-position time-lapse measurement of microfabricated C2C12 populations was programmed in Metamorph software (Molecular Devices) as shown in a previous study [30].

Data analysis

The microscopic images taken were analyzed using the MATLAB image processing toolbox (Mathworks). The particle image velocimetry plug-in is used for the analysis of the velocity field of collective motion. The orientation field was analyzed using a deep-learning-based image processing tool (nematic defect finder) [31] in order to

identify the location and orientation of half-integer topological defects. For particle tracking velocimetry analysis of single cells, single cell nucleus was tracked using TrackMate7.0 [32], and their shapes were detected using Cellpose2.0 [33].

Acknowledgement

We thank K. Kawaguchi (RIKEN), L. Yamauchi (RIKEN) for their technical advice. This work was supported by Grant-in-Aid for Scientific Research on Innovative Areas 18H05427 and 19H05403, Grant-in-Aid for Scientific Research (B) 20H01872, Grant-in-Aid for Challenging Research (Exploratory) from MEXT, and Sumitomo foundation for basic research.

* ymaeda@phys.kyushu-u.ac.jp

- [1] S. Ramaswamy, Annu. Rev. Condens. Matt. Phys. **1**, 323-345 (2010).
- [2] M.C. Marchetti, J.F. Joanny, S. Ramaswamy, T.B. Liverpool, J. Prost, M. Rao, and R.A. Simha, Rev. Mod. Phys. **85**, 1143 (2013).
- [3] T. Vicsek, A. Czirók, E. Ben-Jacob, I. Cohen, and O. Shochet, Physical Review Letters. **75**, 1226 (1995).
- [4] A. Doostmohammadi, J. Ignes-Mullol, J.M. Yeomans, and F. Sagues, Active nematics, Nature Communications **9**, 3246 (2018).
- [5] H. Li, X-q. Shi, M. Huang, X. Chen, M. Xiao, C. Liu, H. Chaté, and H. P. Zhang, Proc. Natl. Acad. Sci. USA **116**, 777-785 (2018).
- [6] Y. I. Yaman, E. Demir, R. Vetter, and A. Kocabas, Nature Communications **10**, 2285 (2019).
- [7] S. J. DeCamp, G. S. Redner, A. Baskaran, M. F. Hagan, and Z. Dogic, Nature Materials **14**, 1110-1115 (2015).
- [8] F. C. Keber, E. Loiseau, T. Sanchez, S. J. DeCamp, L. Giomi, M.J. Bowick, M. C. Marchetti, Z. Dogic, and A. R. Bausch, Science **345**, 1135-1139 (2014).
- [9] C. Blanch-Mercader, V. Yashunsky, S. Garcia, G. Duclos, L. Giomi, and P. Silberzan, Physical Review Letters. **120**, 208101 (2018).
- [10] S-Z. Lin, W-Y. Zhang, D. Bi, B. Li, and X-Q. Feng, Communications Physics **4**, 21 (2021).
- [11] S. P. Thampi, R. Golestanian, and J. M. Yeomans, Physical Review Letters. **111**, 118101 (2013).
- [12] G. Duclos, C. Erlenkamper, J-F. Joanny, and P. Silberzan, Nature Physics **13**, 58-62 (2017).
- [13] T. B. Saw et al., Nature **544**, 212-216 (2017).
- [14] K. Kawaguchi, R. Kageyama, and M. Sano, Nature **545**, 327-331 (2017).
- [15] R. Mueller, J. M. Yeomans, and A. Doostmohammadi, Physical Review Letters. **122**, 048004 (2019).
- [16] Y. Maroudas-Sacks, L. Garion, L. Shani-Zerbib, A. Livshits, E. Braun, and K. Keren, Nature Physics **17**, 251-259 (2021).
- [17] H. Wioland, F. G. Woodhouse, J. Dunkel, J.O. Kessler, and R. E. Goldstein, Physical Review Letters. **110**, 268102 (2013).

- [18] H. Wioland, F. G. Woodhouse, J. Dunkel, and R. E. Goldstein, *Nature Physics* **12**, 341-345 (2016).
- [19] K. Beppu, Z. Izri, J. Gohya, K. Eto, M. Ichikawa, and Y. T. Maeda, *Soft Matter* **13**, 5038-5043 (2017).
- [20] K. Beppu, Z. Izri, T. Sato, Y. Yamanishi, Y. Sumino, and Y. T. Maeda, *Proc. Natl. Acad. Sci. U.S.A.* **118**, e2107461118 (2021).
- [21] D. Nishiguchi, I. Aranson, A. Snezhko, and A. Sokolov, *Nature Communications* **9**, 4486 (2018).
- [22] S. Araki, K. Beppu, A.M.R. Kabir, K. Kakugo, and Y. T. Maeda, *Nano Letters* **21**, 10478-10485 (2021).
- [23] G. Duclos, S. Garcia, H. G. Yevick, and P. Silberzan, *Soft Matter* **10**, 2346-2353 (2014).
- [24] W. Xi, S. Sonam, T. B. Saw, B. Ladoux, and C. T. Lim, *Nature Communications* **8**, 1517 (2017).
- [25] F. J. Segerer, F. Thuroff, A. P. Alberola, E. Frey, and J. O. Rädler, *Physical Review Letters*. **114**, 228102 (2015).
- [26] G. Duclos, C. Blanch-Mercader, V. Yashunsky, G. Salbreux, J.-F. Joanny, J. Prost, and P. Silberzan, *Nature Physics* **14**, 728-732 (2018).
- [27] A. Samui, J. M. Yeomans, and S. P. Thampi, *Soft Matter* **17**, 10640-10648 (2017).
- [28] P. Guillamat, C. Blanch-Mercader, G. Pernellet, K. Kruse, and A. Roux, *Nature Materials* **21**, 588-597 (2022).
- [29] C. Blanch-Mercader, P. Guillamat, A. Roux, and K. Kruse *Physical Review E* **103**, 012405 (2021).
- [30] K. Shigeta, T. Fukuyama, R. Takahashi, K. Beppu, A. Tanaka, and Y.T. Maeda, *RSC Advances* **12**, 20174-20181 (2022).
- [31] Z. Zhou, . Joshi, R. Liu, M. M. Norton, L. Lemma, Z. Dogic, M. F. Hagan, S. Fraden, and P. Hong, *Soft Matter* **17**, 738-747 (2021).
- [32] D. Ersho et al., *Nature Methods* **19**, 829-832 (2022).
- [33] M. Pachitariu and C. Stringer, *Nature Methods* **19**, 1634-1641 (2022).